Proceedings of the IX Bulgarian-Serbian Astronomical Conference: Astroinformatics (IX BSACA) Sofia, Bulgaria, July 2-4, 2014,
Editors: M. K. Tsvetkov, M. S. Dimitrijević, O. Kounchev, D. Jevremović and K. Tsvetkova
Publ. Astron. Soc. "Rudjer Bošković" No 15, 2015, 117-126

MULTI-WAVELENGTH OBSERVATIONS OF AN ERUPTIVE PROMINENCE ON 7 AUGUST 2010

MOMCHIL DECHEV, KOSTADINKA KOLEVA, PETER DUCHLEV and NIKOLA PETROV

Institute of Astronomy, Bulgarian Academy of Sciences
E-mail: mdechev@astro.bas.bg, koleva@astro.bas.bg, duchlev@astro.bas.bg

Abstract. We aim to investigate the morphology and kinematic evolution of a helically-twisted quiescent prominence. The kinematic pattern during the main stages of prominence eruption were studied, using data from both ground-based and space born observatories. The prominence environment and related activity was also considered.

1. INTRODUCTION

The observations show that the eruptive phenomena, such as prominence/filament eruptions, coronal mass ejections (CMEs) and flares are often physically related to each other by the same magnetic flux rope (MFR) occurring in the solar atmosphere (e.g., Gilbert et al. 2000; Gopalswamy et al. 2003; Schrijver et al. 2008; Filippov and Koutchmy 2008). This relation is better expressed between eruptive prominences (EPs) and CMEs. Being one of the earliest known forms of mass ejections from the Sun, EPs started to receive attention in the late 1800s (see Tandberg-Hanssen 1995). Coronagraph observations reveal that CMEs generally have a three-part structure: a bright leading front, a dark cavity, and an inner bright core (e.g. Illing and Hundhausen 1983; Chen et al. 2011). The cavity is usually believed to be a helical flux rope (e.g., Gibson et al. 2006; Riley et al. 2008) and the bright core is thought to be cool prominence/filament matter that is suspended in magnetic dips of a flux rope configuration (e.g., Guo et al. 2010; Jing et al. 2010).

The aforementioned specific physical relationship between EPs and CMEs suggests that the study of the EPs can provide critical clues not only to the prominence activity, but also to the physics of CMEs. Moreover, their study has indicated that the triggering mechanism is related to an unstable MFR (Rubio da Costa et al. 2012 for a review). The observations indicate that the temporal evolution of these phenomena and especially the role played by prominence activation and eruption can be significantly different from event to event (e.g. Sterling and Moore 2005; Wang et al. 2007; Liu et al. 2009; Zuccarello et al. 2009). Therefore, a detailed examination of the kinematic patterns of EP and its triggering mechanism may advance our ability to predict the launch of CME, will the CME be fast or slow etc. Such prediction is

one of the most important subjects in the field of space weather, because the ejections of CMEs from the Sun lead to a significant disturbance of the magnetosphere and affect human technologies and life.

Erupting prominences/filaments are sometimes observed to undergo a rotation about the vertical direction as they rise (e.g. Kliem et al. 2012; Su and van Ballegooijen 2013; Yan et al. 2014 for reviews). Several types of rotating motion of the EP MFR were found out. Rotating magnetic structures driven by underlying photospheric vortex flows were observed by several authors (e.g. Zhang et al. 2011; Wedemeyer - Böhm et al. 2012; Yan et al. 2013). The rotation about the vertical direction and non-radial motion of solar filaments were often observed during their eruptions (e.g. Ji et al. 2003; Green et al. 2007; Jiang et al. 2009; Liu and Alexander 2009; Thompson 2011; Bi et al. 2013). This filament rotation is interpreted as a conversion of twist into writhe in a kink-unstable flux rope. Therefore, MHD helical-kink instability is often taken to be the primary trigger of these eruptions (Fan and Gibson 2007; Török et al. 2010; Kliem et al. 2012). The prominence-related rotation phenomenon was named as giant tornadoes, which were recently concerned due to high-quality observational data of SDO (Li et al. 2012; Su et al. 2012; Wedemeyer et al. 2013; Panesar et al. 2013).

Magnetic reconnection with the ambient field can also cause filament rotation during eruption (Cohen et al. 2010; Thompson 2011). The aforementioned filament rotations should be distinguished from the rotation of the filament around its own axis, namely the "roll effect" (Martin 2003; Panasenco et al. 2011), i.e., the top of the prominence spine gradually bends to one side of the spine during the rise of the filament. This sideways rolling creates twist of opposite sign in the two prominence legs as the prominence continues to rise.

In this paper, we address these issues in analyzing the multi-wavelength observations of an eruptive prominence on 7 August 2010, which showed strong rotational motions during the eruption. We treat an EP and the associated CME as different parts of a flux rope with specific assumed geometrical relationships among the EP, CME, and flux rope. Multi-wavelength observations allow us to investigate the behavior of features of the EP MFR kinematic and geometrical evolution, which helps address whether and in what conditions the eruption of the prominence plays an active role in CME occurrence.

2. OBSERVATIONAL DATA

The eruptive prominence (EP) occurred on the southwestern limb at a mean PA of 255 deg – S15W90 in a quiet Sun region.The observations of the EP on 7 August 2010 used in the present study include the following observations and data.

1. Limb H_α line-center (6563 Å, 1.8 Å bandpass) images by the coronagraph in the National Astronomical Observatory (NAO) - Rozhen, Bulgaria. The resolution of the H-alpha filtergrams is about 2". The images were obtained with a digital camera CANON EOS 350D (8 Mpx). The registered images, at maximal camera resolution, have size of 3456 x 2304 px and one pixel have size of 6.4 x 6.4 μm. The observations of the EP were made between 4:55 UT and 12:47 UT. For this period we have 82 frames. Unfortunately only 21 frames were usable in the time interval 5:05 UT –

12:02 UT. This gives us a bad average cadence of 20 min per frame. The cadence does not allow deriving well kinematic parameters of the eruption and can be used only for illustrative purposes (Fig. 1).

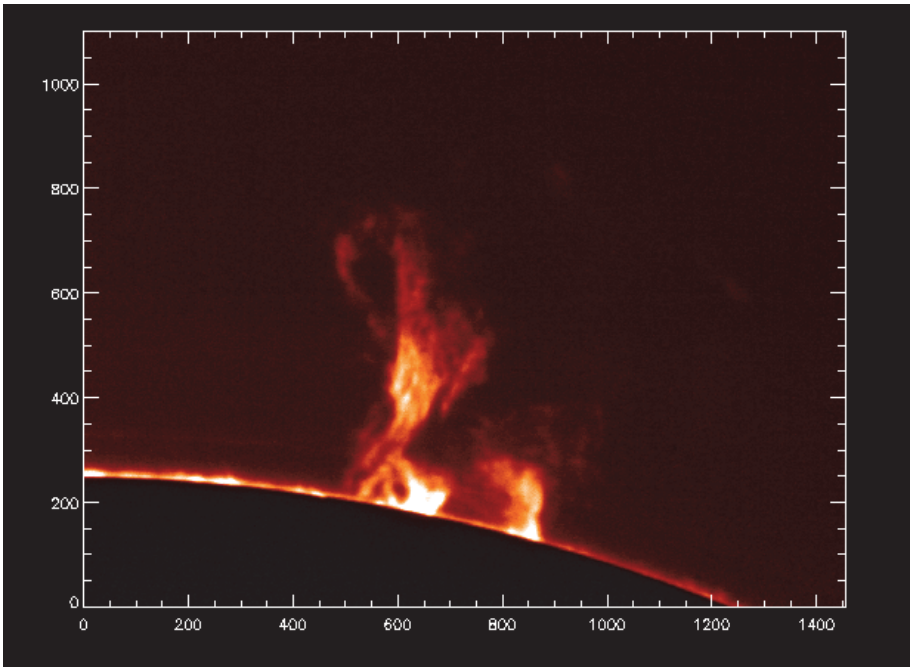

Figure 1: H-alpha image of EP observed at National Astronomical Observatory – Rozhen on 07 August 2010.

2. Full-disk EUV 304 Å high-resolution observations from Solar Dynamics Observatory (SDO: Pesnell et al. 2012)/Atmospheric Imaging Assembly (AIA: Lemen et al. 2012) that provide the opportunity to study the detailed morphological changes in the EP MFR during the development of the EP rotational motion.

3. LASCO C2 white-light coronagraph data (Brueckner et al. 1998) of the Solar and Heliospheric Observatory (SOHO: Brueckner et al. 1995) that cover the range 2-6 solar radii were available for the associated CME.

4. The Extreme-Ultraviolet imager (EUVI: Howard et al. 2008) imaging package onboard the Solar-Terrestrial Relations Observatory (STEREO: Kaiser et al. 2008) also observed this eruption. STEREO-A (Ahead) viewed this event as filament eruption on the solar disk. The separation angle between the twin STEREO spacecraft was about 171°.

2. 1. H-ALPHA

The eruptive prominence (EP) was observed on the southwestern limb at a mean PA of 255 deg – S15W90 in a quiet Sun region. The prominence was observed in National Astronomical observatory – Rozhen by a 15-cm coronagraph with H-alpha filter (1.8 Å bandpass). The resolution of the H-alpha filtergrams is about 2". The images were

obtained with adigital camera CANON EOS 350D (8 Mpx). The registered images, at maximal camera resolution, have size of 3456 x 2304 px and one pixel have size of 6.4 x 6.4 μm.

The observations of the EP were made between 4:55 UT and 12:47 UT. For this period we have 82 frames. Unfortunately only 21 frames were usable in the time interval 5:05 UT – 12:02 UT. This gives us a bad average cadence of 20 min per frame. The cadence does not allow to derive well kinematic parameters of the eruption and can be used only for illustrative purposes (Fig. 1).

2. 2. SDO - AIA

To trace and study the development of the eruption we used the data from SDO (Solar Dynamic Observatory) mission.

SDO mission is part of NASA's Living With a Star (LWS) Program, a program designed to understand the causes of solar variability and its impacts on Earth (http://sdo.gsfc.nasa.gov). SDO supports three scientific experiments:

- Atmospheric Imaging Assembly (AIA);
- EUV Variability Experiment (EVE);
- Helioseismic and Magnetic Imager (HMI);

Each of these experiments performs several measurements, witch show us how and why the Sun varies. The AIA images the solar sphere in multiple wavelengths. Data includes images of the Sun in 10 wavelengths every 10 seconds.

The AIA consists of seven Extreme Ultra-Violet (EUV) and three Ultra-Violet (UV) channels, which provide an unprecedented view of the solar corona with an average cadence of ∼12 s. The AIA image field-of-view reaches 1.3 solar radii with a spatial resolution of ∼1.5". We used level 1 reduced data, i.e. with the dark current removed and the flat-field correction applied. The images were further processed using the standard SolarSoftware procedures.

For the present study we used images (Fig. 2) taken with 1 min cadence in the He II 304 Å and 193 Å passband of AIA/SDO (Lemen et al.,2011). In 193 Å wavelength eruption is not visible and we selected the 304 Å wavelength to work with.

One can see that 304 Å data started 07:30 UT and at ended at 10:59 UT, so a part of the eruption development is not presented.

We also analyzed observations from the Extreme Ultraviolet Imager (EUVI) onboard STEREO Ahead (A) spacecraft. EUVI has a field-of-view of $1.7R_{\odot}$ and observes in four spectral channels (He II 304 Å, Fe IX/X 171 Å, Fe XII 195 Å and Fe XIV 284 Å) that cover the 0.1 to 20 MK temperature range (Wuelser et al., 2004). The EUVI detector has 2048×2048 pixels^2 size and a pixel size of 1.6".

We used images in the He II 304 Å channel with an average cadence of 10 minutes, taken between 07:06 and 12:56 UT.

The separation angle between the two STEREO spacecrafts (A and B) at the time of observation was 150.541 deg.

Images obtained by the Large Angle and Spectrometric Coronagraph (LASCO)/C2 onboard SOHO, whose field-of-view extends from 2 to 6 solar radii (Brueckner, 1995) were also analyzed.

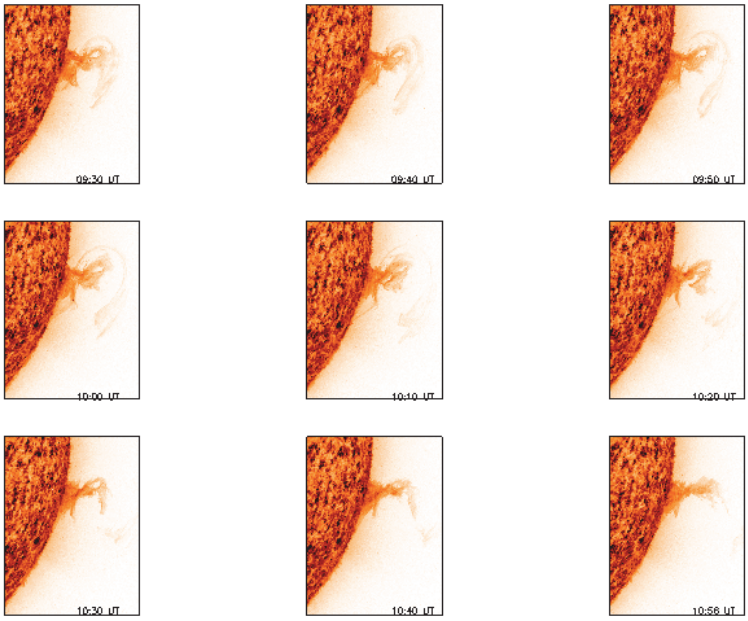

Figure 2: AIA data prominence eruption sequence EP, observed on 07 August 2010 at 304 A. Courtesy of NASA/SDO and the AIA, EVE, and HMI science teams.

3. KINEMATICS

The prominence eruption evolved as a two height-expanding helically twisted magnetic flux ropes with both legs anchored in the quiet Sun region. The main prominence flux ropes was composed of thin magnetic tubes filled with prominence plasma. In the early stages of the eruption the prominence appears to be very dense and one cannot still distinguish any fine structure. During the eruption the prominence body rise and untwist and its small-scale structure becomes visible.

We determined the height of the main prominence flux ropes as well as the height of the projection of the cross point between its legs (Fig. 3). The prominence height was determined as the height of the main axis of the prominence above the visible limb as observed in the He II 304 Å channel of the AIA/SDO images (Fig. 2).

As one can see in the height time diagram (Fig. 4), from 07:31 to 10:59 UT the height of the top prominence loop increase from 180 Mm to 270 Mm with mean velocity of about 8.84 km/s. The velocity was derived with error of $\pm 0.34\ km/s$ from the linear fit of the height-time diagram.

After 10:59 UT the top of the prominence loop quits the AIA FOV During this raising any lift off of the prominence material in to the space was not observed. The prominence eruption was accompanied by a significant untwisting of the main prominence flux ropes.

The height of the bottom prominence loop was measured from 08:30 UT to 10:59 UT. The height-time profile for this part of the prominence body shows similar

behavior as the top loop. The height increase from 190 to 225 Mm with a velocity of about 3.4 km/s (derived with error of ±0.41 km/s).

As regards the projection of the crossing-point of prominence body, it does not change its position during the eruption (Fig. 4).

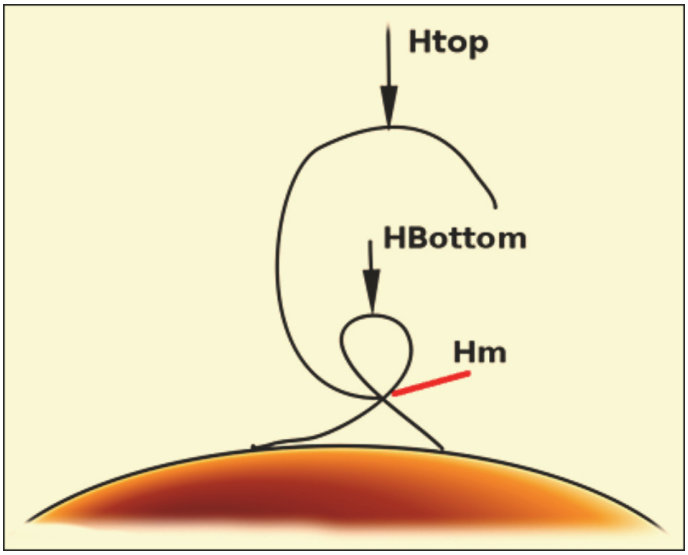

Figure 3: Simple sketch of prominence eruption.

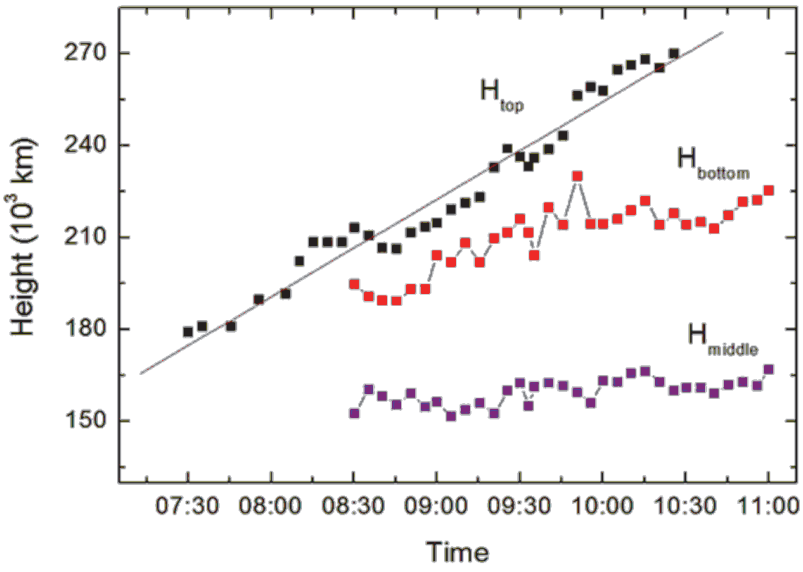

Figure 4: Height-time diagram of the prominence eruption.

4. DISCUSSION

The prominence eruption more often is a result of some kind of instability. A clear sign for magnetohydrodynamic (MHD) instability is the development of helical shape in the course of the eruption (Rust and LaBonte 2005). The Magnetic Flux Rope (MFR) becomes kink-instable when the twist exceeds a critical value of 2π (Hood and Priest 1981, Török and Kleim 2005).

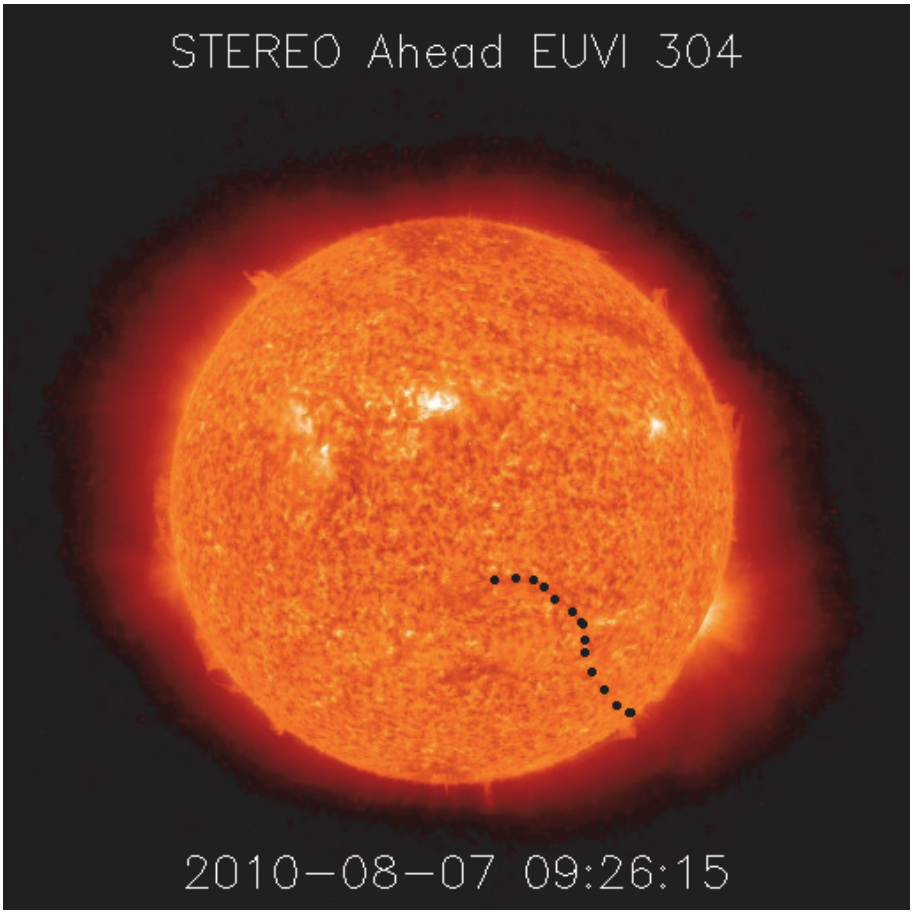

Figure 5: STEREO A/EUVI 304 Å image with traced filament that is the source of the EP on 7 August 2010.

Kink instability was suggested as the trigger of prominence eruption by Sakurai (1976) and later by Török and Kleim (2005) and Fan (2005).

It is difficult to prove observationally the kink instability as a main trigger of prominence destabilization because the helicity can force a flux rope to writhe without any instability occurring (Gilbert et al. 2007 and references therein).

In our case it is well seen on Fig. 1 the helical shape twist of the erupting prominence. So, it is probable that the eruption is due to kink instability. The trigger for development of such instability may be a new emerging flux below the prominence MFR or a propagating disturbance outside the MFR.

There is no sign of new emerging flux in our case, moreover as we see in Fig. 4 the middle point does not change its heights as it should does if an emerging flux push the PMS from below. On the other hand looking at STEREO A/EUVI 304 Å images we can trace the geometrical evolution of the associated filament (Fig. 5) that is the source of the EP at the limb.

The geometrical pattern of the filament and its evolution presented in Figure 6 reveal several specific features of the filament eruption, which throw light on the intricate picture of the EP at the limb.

1. Two neighbor filament segments are undergone eruption. They are located in the eastern part of the filament traced in Figure 5. Therefore, there are two erupted MFRs corresponding of the two filament segments in the event on 7 August 2010.

2. As can see in Figure 6, the MFR of the western segment is located above a part of the eastern one. So, the western MFR correspond to the top one presented in Figure 3, while the eastern MFR correspond to the bottom one in Figure 3.

3. The western MFR erupts more rapidly than the eastern one. At 10:46 UT, when western MFR show well visible kinked loop (Figure 6, central frame), the eastern MFR shows visible rising.

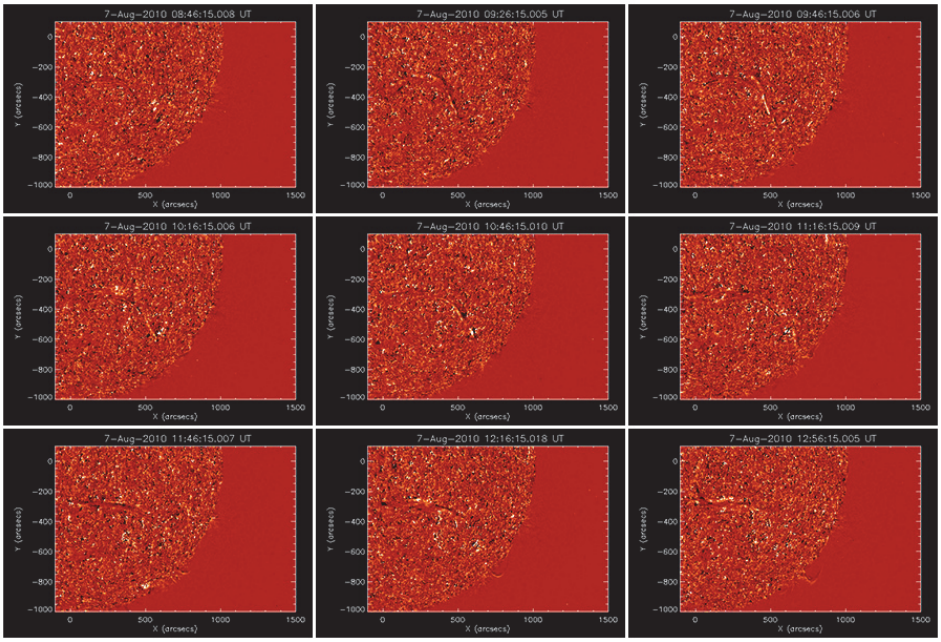

Figure 6: A sample of cropped STEREO A/EUVI 304 Å images showing the evolution of the filament eruption between 09:46 and 12:56 UT.

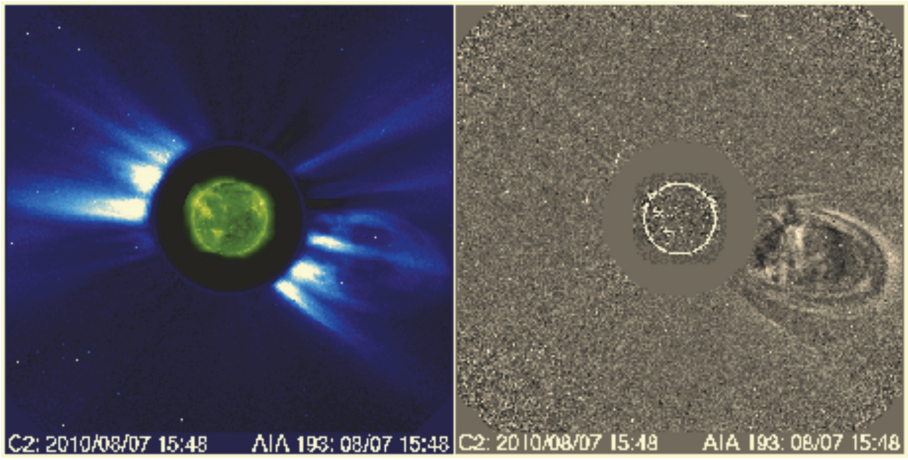

Figure 7: The associated CME, which was registered by LASCO/C2 coronagraph on board on SOHO.

4. At 12:56 UT, when the top of western MFR is escaped the STEREO/EUVI field of view, the eastern MFR shows well visible normal S-shape, which is evident signature for kink-induced process of eruption (Leamon et al. 2003, Kliem et al. 2004, Leka et al. 2005). Moreover, as can see in NAO – Rozhen and SDO/AIA images, at this time the bottom MFR shows well developed kinked loop at the limb. The analysis of the NO)-Rozhen $H\alpha$, SDO/AIA 304 A, and STEREOA/EUVI 304 Å data reveal an interesting case of two neighbor filament segments eruption. One of them (western) actively participates in the eruptive evolution of the large-scale MFR that produce CME (Figure 7). Another one (eastern MFR) shows behavior of confined eruption. The superimposing of the projections of these two MFRs on the sky plane creates the intricate picture of the EP on 7 August 2014 at the limb.

The EP was associated with a large CME, which was registered by LASCO/C2 coronagraph on board on SOHO. The CME first appearance in C2 field of view was in 11:00 UT. The CME was centered in PA of 250 deg, and propagated with average linear speed of 288 km/s.

Acknowledgements

The authors are grateful to SDO/AIA, SOHO/LASCO, and STEREO/EUVI teams for providing the wonderful data.

References

Bi, Y., Jiang, Y., Yang, J., Zheng, R., Hong, J., Li, H., Yang, D., Yang, B.: 2013, *ApJ*, **773**, 162.
Brueckner, G. E., et al.: 1995, *Sol. Phys.*, **162**, 357.
Bruekner, G. E., et al.: 1998,*Geophys. Res. Lett.*, **25**, 3019.
Cheng, X., Zhang, J., Liu, Y., Ding, M. D.: 2011, *ApJL*, **732**, 25.
Cohen, O., Attrill, G. D. R., Schwadron, N. A., et al.: 2010, *JGRA*, **115**, 10104.
Fan, Y., Gibson, S. E.: 2007, *ApJ*, **668**, 1232.
Fan, Y.: 2005, *ApJ*, **630**, 543.

Filippov, B. P., Koutchmy, S.: 2008, *Ann. Geophys.*, **26**, 3025.
Gibson, S. E., Foster, D., Burkepile, J., de Toma, G., Stanger, A.: 2006, *ApJ*, **641**, 590.
Gilbert, H. R, Alexander, D., Liu, R.: 2007, *Sol. Phys.*, **245**, 287.
Gilbert, H. R., Holzer, T. E., Brukerile, J. T., Hundhausen, A. J.: 2000, *ApJ*, **537**, 503.
Gopalswamy, N., Shimojo, M., Lu, W., et al.: 2003, *ApJ*, **586**, 562.
Green, L. M., Kliem, B., Török, T., van Driel-Gesztelyi, L., Attrill, G. D. R.: 2007, *Sol. Phys.*, **246**, 365.
Guo, Y., Schmieder, B., Démoulin, P., et al.: 2010, *ApJ*, **714**, 343.
Hood, A. W., Priest, E. R.: 1981, *Geophys. Astrophys. Fluid Dyn.*, **17**, 297.
Howard, R. A., Moses, J. D., Vourlidas, A., et al.: 2008, *Space Sci. Rev.*, **136**, 67.
Illing, R. M. E., Hundhausen, A. J.: 1983, *JGR*, **88**, 10210.
Ji, H., Wang, H., Schmahl, E. J., Moon, Y. J., Jiang, Y.: 2003, *ApJ*, **695**, L135.
Jiang, Y., Yang, J., Zheng, R., Bi, Y., Yang, X.: 2009, *ApJ*, **693**, 1851.
Jing, J., Yuan, Y., Wiegelmann, T., et al.: 2010, *ApJL*, **719**, 56.
Kaiser, M. L., Kucera, T. A., Davila, J. M., et al.: 2008, *Space Sci. Rev.*, **136**, 5.
Kliem, B., Török, T., Thompson, W. T.: 2012, *Sol. Phys.*, **281**, 137.
Kliem, B., Titov, V. S., Török, T.: 2004,*A&A*, **413**, L23.
Leamon, R. J., Canfield, R. C., Blehm, Z., Pevtsov, A. A.: 2003, *ApJ*, **596**, L255.
Leka, K. D., Fan, Y., Barnes, G.: 2005, *ApJ*, **626**, 1091.
Lemen, J. R., Title, A. M., Akin, D. J., et al.: 2012, *Sol. Phys.*, **275**, 17.
Lemen, J. R., Title, A. M., Akin, D. J. et al.: 2011, *Sol.Phys.*, **172**.
Li, X., Morgan, H., Leonard, D., Jeska, L.: 2012, *ApJ*, **752**, L22.
Liu, C., Lee, J., Karlický, M., Prasad Choudhary, D., Deng, N., Wang, H.: 2009, *ApJ*, **703**, 757.
Liu, R., Alexander, D.: 2009, *ApJ*, **697**, 999.
Martin, S. F.: 2003, *AdSpR*, **32**, 1883.
Panasenco, O., Martin, S., Joshi, A. D., Srivastava, N.: 2011, *JASTP*, **73**, 1129.
Panesar, N. K., Innes, D. E., Tiwari, S. K., Low, B. C.: 2013, *A&A*,**549**, 105.
Pesnell, W. D., Thompson, B. J., Chamberlin, P. C.: 2012, *Sol. Phys.*, **275**, 3.
Riley, P., Lionello, R., Mikić, Z., Linker, J.: 2008, *ApJ*, **672**, 1221.
Rubio da Costa, F., Zuccarello, F., Fletcher, L., Romano, P., Labrosse, N.: 2012, *A&A*, **539**, 27.
Rust, D. M., LaBonte, B. J.: 2005, *ApJ*, **622**, L69.
Sakurai, T.: 1976, *PASJ*, **28**, 177.
Schrijver, C. J., Elmore, C., Kliem, B., Török, T., Trrle, A. M.: 2008, *ApJ*, **674**, 586.
Sterling, A. C., Moore, R. L.: 2005, ApJ, **630**, 1148.
Su, Y. ,Wang, T., Veronig, A., Temmer, M., Gan, W.: 2012, *ApJ*, **756**,41.
Su, Yingna, van Ballegooijen, Adriaan: 2013, *ApJ*, **764**, 91.
Tandberg-Hanssen, E.: 1995, The Nature of Solar Prominences (Dordrecht: Kluwer)
Thompson, W. T.: 2011, *JASTP*, **73**, 1138.
Török, T., Berger, M. A., Kliem, B.: 2010, *A&A*, **516**, 49.
Török, T., Kliem, B.: 2005, *ApJ*, **630**, L97.
Wang, H., Liu, C., Jing, J., Yurchyshyn, V.: 2007, *BAAS*, **38**, 214.
Wedemeyer - Böhm, S., Scullion, E., Steiner, O., Rouppe van der Voort, L., et al.: 2012, *Nature*, **486**, 505.
Wedemeyer, S., Scullion, E., Rouppe van der Voort, Luc, Bosnjak, A., Antolin, P.: 2013, *ApJ*, **774**, 123.
Wuelser, J.-P., Lemen, J. R., Tarbell, T. D, et al.,: 2004, in **SPIE Conf.**, ed. S. Fineschi & M. A. Gummin, **5171**, 111.
Yan, X. L., Pan, G. M., Liu, J. H., Qu, Z. Q., Xue, Z. K., Deng, L. H., Ma, L., Kong, D. F.: 2013, *AJ*, **145**, 153.
Yan, X. L., Xue, Z. K., Liu, J. H., Ma, L., Kong, D. F., Qu, Z. Q., Li, Z.: 2014, *ApJ*, **782**, 67.
Zhang, J., Liu, Y.: 2011, ApJ, **741**, L7.
Zuccarello, F., Romano, P., Farnik, F., Karlický, M., et al.: 2009, *A&A*, **493**, 629.